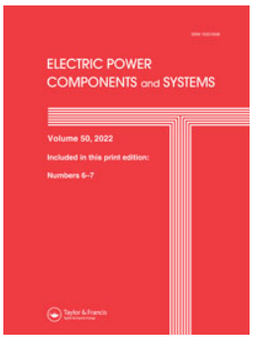

Taylor & Francis
Taylor & Francis Group

Electric Power Components and Systems

ISSN: 1532-5008 (Print) 1532-5016 (Online) Journal homepage: www.tandfonline.com/journals/uemp20

Enhanced Weighting Factor Eliminated Predictive Torque Control of an Open End Winding Induction Motor Drive

V. Praveen Kumar Kunisetti & T. Vinay Kumar

To cite this article: V. Praveen Kumar Kunisetti & T. Vinay Kumar (2022) Enhanced Weighting Factor Eliminated Predictive Torque Control of an Open End Winding Induction Motor Drive, Electric Power Components and Systems, 50:6-7, 318-330, DOI: 10.1080/15325008.2022.2136294

To link to this article: https://doi.org/10.1080/15325008.2022.2136294

Electric Power Components and Systems, 50(6-7): 318–330, 2022

ISSN: 1532-5008 print / 1532-5016 online
DOI: 10.1080/15325008.2022.2136294

Enhanced Weighting Factor Eliminated Predictive Torque Control of an Open End Winding Induction Motor Drive

V. Praveen Kumar Kunisetti [1] and T. Vinay Kumar [2]
[1]Department of Electrical Engineering, Sardar Vallabhbhai National Institute of Technology, Surat, India
[2]Department of Electrical Engineering, National Institute of Technology, Warangal, India

CONTENTS

Abstract—Predictive torque control (PTC) of induction motor drives is one of the best suitable alternatives for direct torque control (DTC). In this article, the weighting factor eliminated PTC for four-level inversion fed open end winding induction motor drive (OEWIMD) has been introduced. The major limitations of classical PTC are as follows: assignment of weighting factor due to dissimilar control objectives, tuning of weighing factors and high computational burden. To circumvent these problems, this article introduces an effective weighting factor elimination-based PTC scheme to an OEWIMD. The proposed algorithm eliminates the complex tuning process of weighting factors by classifying the cost function. The proposed PTC algorithm is simple and provides less computational burden on the controller. In the proposed PTC, the cost function is segregated and ranked accordingly to reduce flux and torque ripples. Cost function-I is formulated to obtain optimum voltage vectors to reduce flux ripples. The same voltage vectors obtained from cost function-I are used in cost function-II to maintain minimum torque ripple. Therefore, the proposed PTC reduces torque and flux ripples with a limited number of voltage vectors and maintains minimum computational burden. The effectiveness of the proposed PTC is verified through MATLAB/SIMULINK and experimentation.

Keywords: dual inverter configuration, four-level inversion, flux control, open end winding induction motor drives, predictive torque control and weighting factor elimination

Received 9 September 2021; accepted 12 June 2022

Address correspondence to V. Praveen Kumar Kunisetti, Department of Electrical Engineering, Sardar Vallabhbhai National Institute of Technology, Surat, India. E-mail: Kvpraveenkumar15@gmail.com

1. INTRODUCTION

Variable speed drives (VSDs) are more pronounced in case of Industrial drives and Electrical Vehicles (EVs). VSDs with Induction Motor drives are used in many industrial applications and also in EVs. In recent days, many of the VSDs are employed with multi-level inverters (MLIs). The MLI configurations can provide a large number of voltage vectors, which in turn gives precise control and reduces ripples in torque and flux [1]. In the literature [2], there are several MLI configurations, apart from these MLI configurations dual inverter fed open-end winding induction motor drive (OEWIMD) provides several benefits such as: (i) it gives multi-level inversion by using two inverters in dual mode, (ii) clamping diodes are not needed, these are used

in neutral point clamped (NPC) inverters, (iii) high in redundancy of switching states, (iv) it operates with less capacitors as compared to flying capacitor MLIs and (v) it uses few DC sources as involved in cascaded H-Bridge MLIs (CHB-MLI). The OEWIMD became popular, due to its potential applications like ship propulsion, electric vehicles and renewable energy interfacing [3].

The speed control of VSDs can be done by various control algorithms [4]. For high-dynamic performance applications Field Oriented Control (FOC) and Direct Torque Control (DTC) are preferred. The scheme of DTC uses hysteresis controllers, the control in a stationary reference frame and do not use modulator [5]. DTC has several advantages; however, there exists certain limitations for classical DTC. The limitations in classical DTC are the use of hysteresis boundaries causes variable switching frequency, problems during startup and low speeds, complex switching state tables for MLIs and higher ripples in torque and flux. In order to reduce the torque ripple and also to maintain constant switching frequency, modulated hysteresis control using space vector modulation (SVM) has been introduced for a two-level inverter-fed induction motor drive [6]. Some of the problems in DTC can be easily handled by another promising technology known as predictive torque control (PTC) or Finite Control Set Predictive Torque Control (FCS-PTC). The scheme of PTC combines the features of model predictive control (MPC) and DTC. MPC has several advantages: ease of implementation, inclusion of constraints into cost function and simple control algorithms [7]. PTC uses discrete models of power circuit and VFD. The discrete models are used for prediction of control variables and minimization of cost function. The switching state which gives a minimum value of cost function is termed as the optimal voltage vector and it is applied to inverter in sequential control cycle. The cost function used in classical PTC consists of torque and flux error minimization. If the cost function comprises dissimilar terms, the weighting factors is unavoidable. The tuning of these weighting factors is quite difficult. Nevertheless, PTC also has several limitations [8, 9]: (i) it operates with variable switching frequency, (ii) higher ripples in torque and flux, (iii) cumbersome tuning of weighting factors and (iv) higher computational burden.

In the recent past, various researchers came up with their analytics to address the limitations of classical PTC. In [10], PTC of induction motor with discrete space phasor modulation has been proposed to reduce the computational burden and also to maintain constant switching frequency; this method does not create any sub-optimization issues during both steady state and transient modes. In [11, 12] duty cycle control-based PTC with extended set of voltage vectors has been introduced to reduce ripples in torque and flux. The performance of motor drive has been improved [11, 12], whereas the problem of weighting factors, switching frequency issues and computational complexity are not solved. In [13], PTC of induction motor has been developed for fault tolerant with four switch three-phase inverter topology. It utilizes discrete space vector modulation and also presents mathematical relations in fault tolerant control PTC strategy. In order to eliminate the weighting factors, two individual cost functions are used and their results are cascaded to obtain an optimal voltage vector [14]. For stable operation, field weakening strategy and generalized sequential model predictive control have been used. This method has been applied for a two-level inverter-fed induction motor, and it contains less number of switching states [14]. In the recent past, several researchers initiated weighting factor elimination strategies for classical two-level three-phase inverter-fed motor drives [15, 16]. In [15], the weighting factors are eliminated by calculating the torque boundaries and evaluating the cost function with flux error. The cost function in terms of flux eliminates the weighting factor, and it is also known that stator flux vector can be converted into stator voltage vectors [16], a modified cost function has been used in terms of stator voltage vectors to reduce computational burden and weighting factors tuning process.

For medium power applications, the preferable alternative is MLI-fed induction motor drives. PTC of MLI-fed induction motor drives has been introduced [17–24]. In [17, 18], PTC of OEWIMD with four-level inversion has been introduced. PTC of OEWIMD has been introduced with a limited number of voltage vectors by classifying them into different groups [17]. In [18], predictive angle-based PTC has been developed for an OEWIMD. The limitation of this method is the accuracy of angle prediction depends on parameters of the motor drive. To address the computational burden, the application of voltage vectors used for prediction is reduced by using the position of stator flux and its deviation from the reference [19], but it requires pre-selection of voltage vectors based on the position of stator flux by classifying flux trajectory into sectors. To eliminate the weighting factors, and also to maintain a constant neutral point voltage, a two-stage flux optimization-based PTC has been introduced [20]. The use of two-stage flux optimization stage and calculation of reference flux vector require more accurate estimation of rotor angle and the computational burden will also increase. In

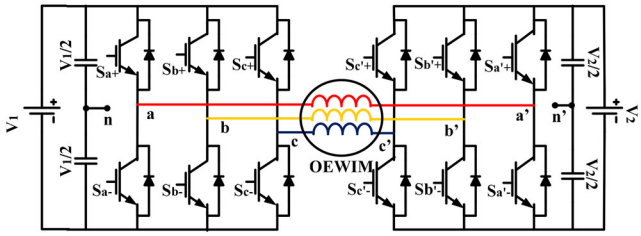

FIGURE 1. Configuration of dual inverter fed OEWIMD.

[21], vector partition-based torque control is introduced to eliminate the weighting factors. It requires stator flux position and a predetermined set of voltage vectors. PTC of OEWIMD, with elimination of weighting factors based on ranking has been performed [22], by evaluating the cost function for all voltage vectors. For an OEWIMD to eliminate the weighting factors, a simplified PTC has been introduced with electromagnetic torque and reactive torque components into the cost function [23]. In order to reduce the computational burden on controller nearest voltage vector scheme has been applied. It requires additional PI controller as compared to classical PTC and also requires an algorithm to find the nearest voltage vector. In [24], to eliminate the weighting factor reference stator flux vector calculation has been performed to eliminate weighting factors and information on flux space phasor has been used to reduce the computational burden. In [25, 26] and [27], non-linear model predictive control techniques have been introduced for an hybrid system with repetitive disturbances, constrained and unconstrained systems in the presence of disturbance and the presence of uncertainty are proposed. The methods introduced in [25–27] are used for non-linear systems in real time applications.

This article focuses on the implementation of PTC strategy to an OEWIMD with four-level inversion. The OEWIMD has several advantages over other Multi-level inverter fed Induction motor drives and those are as follows: It requires two two-level inverters to obtain four-level output voltage. Clamping diodes are not required, neutral voltage fluctuations are absent, offers high redundancy in voltage space vectors, it requires smaller number of capacitors as compared to other topologies, ease of control, requires less number of DC supplies as compared to cascaded H-bridge topologies and it has the capability to operate in faulty conditions. The following are limitations of OEWIMD configuration: There may be problems due to common-mode voltage and require more number of gate pulses as compared to conventional two-level inverter fed Induction Motor Drive. Classical PTC of OEWIMD has been developed by considering all possible space vector locations of an inverter. In a dual inverter fed OEWIMD there exist '64' switching combinations and these combinations provide '37' active space vector locations. These '37' space vector locations are considered to maintain less common-mode voltage (CMV) and less number of switching transitions. In this article PTC of OEWIMD is developed by classifying the cost function into two terms in order to eliminate weighting factors. The cost function-I is used to reduce flux errors and the voltage vectors that provides minimum values of cost function-I are used in cost function-II. The second cost function comprises torque error and the voltage vectors that give the minimum value of cost function-II are used to obtain the optimal voltage vector. In order to verify the effectiveness of the developed weighting factor eliminated PTC strategy, it is implemented in MATLAB and performed by experimentation. The obtained experimental results are compared with classical PTC and compared with recent PTC techniques. In order to compare simulation and experimental results, articles [22] and [24] are used. In [22] and [24] weighting factors are eliminated by assuming flux space phasor. These methods [22, 24] are quite complex because these methods use sector information, trigonometric function and predefined set of voltage vectors.

2. DUAL INVERTER FED OEWIMD CONFIGURATION

2.1. Dual Inverter Configuration

The dual inverter configuration is shown in Figure 1. It uses two two-level Voltage Source Inverters (VSI) for its operation and the two inverters are operated with unequal DC-link voltage (asymmetrical configuration). The two inverters are operated with DC-link voltages of 2:1 ratio thereby the dual inverter configuration provides four-level inversion. The two inverters are operated with V_1 (voltage of inverter-I) and V_2 (voltage of inverter-II), where $V_1 = (2V_{dc}/3)$ and $V_2=(V_{dc}/3)$. Net DC-link voltage (V_{dc}) is $V_{dc}=V_1+V_2$.

The pole voltages of inverter-I are shown in (1) and these are mentioned as V_{an}, V_{bn} and V_{cn}. The pole voltage of inverter-II is given by (2), and these are denoted as $V_{a'n'}$, $V_{b'n'}$ and $V_{c'n'}$. The difference in pole voltages is given by (3). From the difference of pole voltages ($\delta V_{aa'}$, $\delta V_{bb'}$,$\delta V_{cc'}$), the CMV (V_c) has been evaluated and it is given by (4).

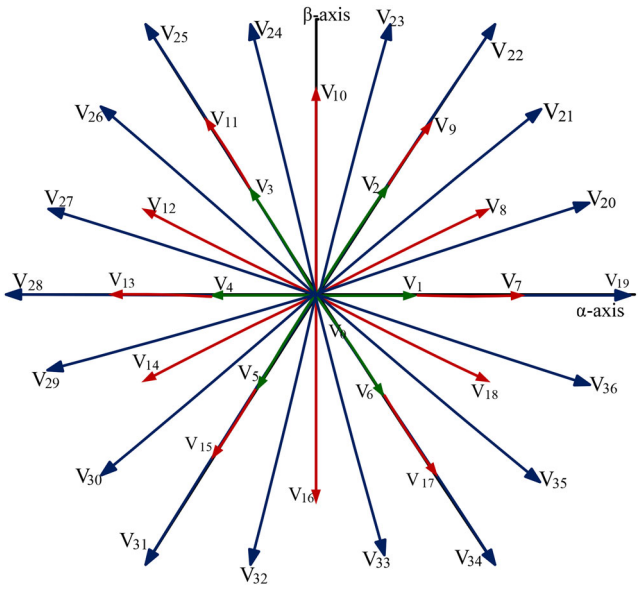

FIGURE 2. Voltage space vectors of dual inverter fed OEWIMD.

$$\begin{bmatrix} V_{an} \\ V_{bn} \\ V_{cn} \end{bmatrix} = \begin{cases} \dfrac{V_1}{2} & when \quad S_a = S_b = S_c = 1 \\ -\dfrac{V_1}{2} & when \quad S_a = S_b = S_c = 0 \end{cases} \tag{1}$$

$$\begin{bmatrix} V_{a'n'} \\ V_{b'n'} \\ V_{c'n'} \end{bmatrix} = \begin{cases} \dfrac{V_2}{2} & when \quad S_{a'} = S_{b'} = S_{c'} = 1 \\ -\dfrac{V_2}{2} & when \quad S_{a'} = S_{b'} = S_{c'} = 0 \end{cases} \tag{2}$$

$$\begin{bmatrix} \delta V_{aa'} \\ \delta V_{bb'} \\ \delta V_{cc'} \end{bmatrix} = \begin{bmatrix} V_{an} - V_{a'n'} \\ V_{bn} - V_{b'n'} \\ V_{cn} - V_{c'n'} \end{bmatrix} \tag{3}$$

$$V_c = (1/3)(\delta V_{aa'} + \delta V_{bb'} + \delta V_{cc'}) \tag{4}$$

From the difference of pole voltages (3) and CMV (4), the phase voltages ($V_{aa'}$, $V_{bb'}$, $V_{cc'}$) are obtained and it is given by (5) whereas (6) represents a simplified form of phase voltage.

$$\begin{bmatrix} V_{aa'} \\ V_{bb'} \\ V_{cc'} \end{bmatrix} = \begin{bmatrix} \delta V_{aa'} \\ \delta V_{bb'} \\ \delta V_{cc'} \end{bmatrix} - \begin{bmatrix} V_c \\ V_c \\ V_c \end{bmatrix} \tag{5}$$

$$\begin{bmatrix} V_{aa'} \\ V_{bb'} \\ V_{cc'} \end{bmatrix} = (1/3) \begin{bmatrix} 2 & -1 & -1 \\ -1 & 2 & -1 \\ -1 & -1 & 2 \end{bmatrix} \begin{bmatrix} \delta V_{aa'} \\ \delta V_{bb'} \\ \delta V_{cc'} \end{bmatrix} \tag{6}$$

Figure 2 represents active voltage space vectors of dual inverter-fed OEWIMD. The voltage space vectors of inverter-1 (V_{s1}) and inverter-2 (V_{s2}) are given by (7), (8). The voltage space vector of the dual inverter configuration is given by (9).

$$V_{s1} = \left(\frac{2}{3}\right)(V_1)\left(S_a + S_b e^{j2\pi/3} + S_c e^{j4\pi/3}\right) \tag{7}$$

$$V_{s2} = \left(\frac{2}{3}\right)(V_2)\left(S_{a'} + S_{b'} e^{j2\pi/3} + S_{c'} e^{j4\pi/3}\right) \tag{8}$$

The resultant voltage space vector (V_s) (14) is obtained from the difference of (12) and (13).

$$V_s = V_{s1} - V_{s2} \tag{9}$$

The realization of voltage space vectors and their switching combinations for four-level inversion is shown in [3] and [22]. Voltage space vector locations are obtained from switching combinations of Inverter-1 and Inverter-2.

2.2. Dynamic Model of OEWIM

The discrete/dynamic model of OEWIMD is developed in stationary reference frames (Clarke's transformation). The discrete model of OEWIMD is used for the estimation and predictive of control variables (flux and torque). The stator and rotor voltage equations of OEWIMD are given by (10) and (11).

$$\begin{pmatrix} V_{s\alpha}(k) \\ V_{s\beta}(k) \end{pmatrix} = R_s \begin{pmatrix} i_{s\alpha}(k) \\ i_{s\beta}(k) \end{pmatrix} + p \begin{pmatrix} \psi_{s\alpha}(k) \\ \psi_{s\beta}(k) \end{pmatrix} \tag{10}$$

$$\begin{pmatrix} 0 \\ 0 \end{pmatrix} = R_r \begin{pmatrix} i_{r\alpha}(k) \\ i_{r\beta}(k) \end{pmatrix} + p \begin{pmatrix} \psi_{r\alpha}(k) \\ \psi_{r\beta}(k) \end{pmatrix} + \omega_r \begin{pmatrix} \psi_{r\beta}(k) \\ -\psi_{r\alpha}(k) \end{pmatrix} \tag{11}$$

The stator and rotor flux is given by (12) and (13). From (10)–(13), the electromagnetic torque of OEWIMD can be obtained (14).

$$\begin{pmatrix} \psi_{s\alpha}(k) \\ \psi_{s\beta}(k) \end{pmatrix} = L_s \begin{pmatrix} i_{s\alpha}(k) \\ i_{s\beta}(k) \end{pmatrix} + L_m \begin{pmatrix} i_{r\alpha}(k) \\ i_{r\beta}(k) \end{pmatrix} \tag{12}$$

$$\begin{pmatrix} \psi_{r\alpha}(k) \\ \psi_{r\beta}(k) \end{pmatrix} = L_r \begin{pmatrix} i_{r\alpha}(k) \\ i_{r\beta}(k) \end{pmatrix} + L_m \begin{pmatrix} i_{s\alpha}(k) \\ i_{s\beta}(k) \end{pmatrix} \tag{13}$$

$$T(k) = \left(\frac{3}{2}\right)\left(\frac{P}{2}\right)\left(\psi_{s\alpha}(k) i_{s\beta}(k) - \psi_{s\beta}(k) i_{s\alpha}(k)\right) \tag{14}$$

The speed of OEWIMD is estimated by using (15) [3] and [22].

$$J\frac{d\omega_m}{dt} = T(k) - T_l \tag{15}$$

In (10) to (15), stator voltages, flux and currents are $V_{s\alpha}(k)$, $V_{s\beta}(k)$, $\psi_{s\alpha}(k)$, $\psi_{s\beta}(k)$ and $i_{s\alpha}(k)$, $i_{s\beta}(k)$, respectively. Rotor currents are $i_{r\alpha}(k)$, $i_{r\beta}(k)$. Rotor flux is $\psi_{r\alpha}(k)$, $\psi_{r\beta}(k)$. Stator and Rotor resistances are R_s and R_r. Stator and Rotor inductances are L_s and L_r. The number of poles of OEWIM is P and the differential operator is p. The

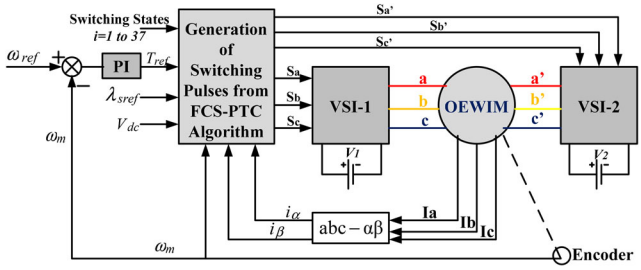

FIGURE 3. Block diagram of classical PTC.

electromagnetic torque and load torque is $T(k)$ and T_l. The motor speed is ω_m.

3. PROPOSED WEIGHTING FACTOR ELIMINATION-BASED PTC STRATEGY

3.1. Classical PTC

The block diagram of classical PTC is shown in Figure 3. Classical PTC of OEIWM was implemented by considering 37 possible space vector locations of dual inverter configuration [22]. If the voltage space vectors and their realizations are known, then it is easy to develop the PTC algorithm. PTC works on the following steps:

Step 1: Estimation of flux at kth instant with the help of voltage and current measurements (10).

Step 2: If the flux is estimated, then with the help of flux at kth instant, flux at $(k+1)$ is predicted (16). By using flux, current at $(k+1)$ instant (16), (18); torque is estimated at $(k+1)$ instant (19). The derivation of torque at $(k+1)$ instant is clearly described in [17, 22].

Step 3: With the help of torque and flux at $(k+1)$ instant cost function is formulated (20).

Step 4: The cost function is evaluated for all 37 combinations of voltage space vectors and the switching state which gives the minimum cost function is known as optimum voltage vector and it is applied in the next control cycle.

$$\begin{pmatrix}\lambda_{s\alpha}(k+1)\\ \lambda_{s\beta}(k+1)\end{pmatrix} = T_s\left(\begin{pmatrix}V_{s\alpha}(k)\\ V_{s\beta}(k)\end{pmatrix} - R_s\begin{pmatrix}i_{s\alpha}(k)\\ i_{s\beta}(k)\end{pmatrix}\right) + \begin{pmatrix}\lambda_{s\alpha}(k)\\ \lambda_{s\beta}(k)\end{pmatrix} \tag{16}$$

$$\begin{pmatrix}\lambda_{r\alpha}(k)\\ \lambda_{r\beta}(k)\end{pmatrix} = A\begin{pmatrix}\lambda_{s\alpha}(k)\\ \lambda_{s\beta}(k)\end{pmatrix} + B\begin{pmatrix}i_{s\alpha}(k)\\ i_{s\beta}(k)\end{pmatrix} \tag{17}$$

$$\begin{pmatrix}i_{s\alpha}(k+1)\\ i_{s\beta}(k+1)\end{pmatrix} = T_s\begin{pmatrix}E\begin{pmatrix}\psi_{r\alpha}(k)\\ \psi_{r\beta}(k)\end{pmatrix} - F\begin{pmatrix}i_{s\alpha}(k)\\ i_{s\beta}(k)\end{pmatrix}\\ +G\begin{pmatrix}\psi_{r\beta}(k)\\ -\psi_{r\alpha}(k)\end{pmatrix} + \frac{1}{D}\begin{pmatrix}V_{s\alpha}(k)\\ V_{s\beta}(k)\end{pmatrix}\end{pmatrix} + \begin{pmatrix}i_{s\alpha}(k)\\ i_{s\beta}(k)\end{pmatrix} \tag{18}$$

$$T(k+1) = \frac{3}{2}\frac{P}{2}\left(\lambda_{s\alpha}(k+1)i_{s\beta}(k+1) - \lambda_{s\beta}(k+1)i_{s\alpha}(k+1)\right) \tag{19}$$

$$g = \sigma_T\left|T_{ref} - T(k+1)\right| + \sigma_\psi\left|\lambda_{sref} - \lambda_s(k+1)\right| \tag{20}$$

Where

$A = \frac{L_r}{L_m}, B = \left(L_m - \frac{L_sL_r}{L_m}\right), C = \left(\frac{L_mR_r}{L_r}\right), D = \left(\frac{L_sL_r - L_m^2}{L_r}\right),$
$E = \left(\frac{L_mR_r}{L_r^2D}\right), F = \frac{L_m}{L_rD}\left(\frac{L_mR_r}{L_r} + \frac{R_sL_r}{L_m}\right)$ and $G = \left(\frac{L_m}{L_rD}\right)$.

In (20), σ_T and σ_ψ are known as torque and flux weighting factors. The selection of these weighting factors affects the performance of OEWIMD. There is no particular method to select weighting factors; various researchers came up with their thoughts to simplify these weighting factors [12, 17, 22]. The torque ripple, flux ripple associated with classical PTC is also high. In order to reduce the ripples in torque, flux and also to eliminate the effect of weighting factors, this article introduces a simple weighting factor eliminated PTC strategy to OEWIMD.

3.2. Simplified Weighting Factor Eliminated PTC

The block diagram of the weighting factor elimination-based PTC strategy is shown in Figure 4. The proposed PTC strategy works in a similar way to the conventional PTC strategy. The proposed PTC strategy utilizes the operating speed of the motor that is taken from the encoder of the motor, the voltage vectors corresponding to all switching combinations, the phase currents of the motor obtained from current sensors, and the DC link voltage of the inverter obtained from voltage sensors. With the help of DC-link voltage, the voltage vectors required for the operation of OEWIMD are obtained. The measured phase currents and phase voltages are used to estimate the flux of the OEWIMD and The flux prediction, currents prediction and torque predictions are obtained by using (16), (18) and (19). With the help of the operating speed, predicted flux and torque of the OEWIMD, the cost function has been formulated. The proposed cost function utilizes splitting of

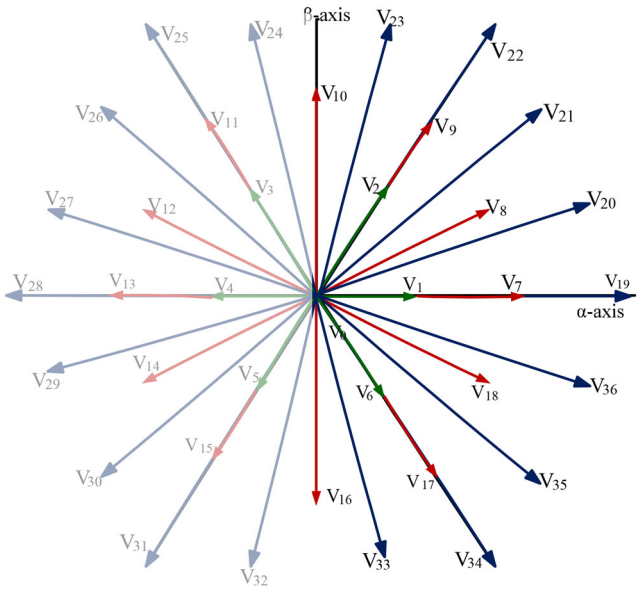

FIGURE 5. Voltage space vectors used to increase or decrease flux ripple by assuming flux space vector in sector-1.

the cost function used in conventional PTC (20). The working model of the proposed PTC is as follows.

The algorithm used to implement this strategy is as follows:

Step 1: Estimate flux at k^{th} instant for all 37 voltage space vector combinations of dual inverter configuration by using current measurement and realization of voltage space vectors.

Step 2: Predict the flux at $(k+1)$ instant by using (16) for 37 voltage space vector locations.

Step 3: Formulate cost function g_1 by using $\lambda_s(k+1)$, λ_{sref}.

Step 4: Evaluate the cost function g_1 and arrange the first 20 minimum values of the cost function with their switching state combinations.

$$g_1 = \left|\lambda_{sref} - \lambda_s(k+1)\right| \tag{21}$$

Step 5: Store the first 20 voltage space vector combinations and $\lambda_s(k+1)$ for those switching combinations in a ranked manner.

Step 6: Predict current at $(k+1)$ instant by using (18) for the switching combinations obtained in step 4.

Step 7: By using current and flux obtained in Step 5 and Step 6 and predict Torque at $(k+1)$ instant (19).

Step 8: Formulate cost function g_2, with the help of $T(k+1)$ and T_{ref}.

$$g_2 = \left|T_{ref} - T(k+1)\right| \tag{22}$$

Step 9: Minimize cost function g_2 and also store the voltage vectors which give less torque ripple that are arranged in a ranked manner.

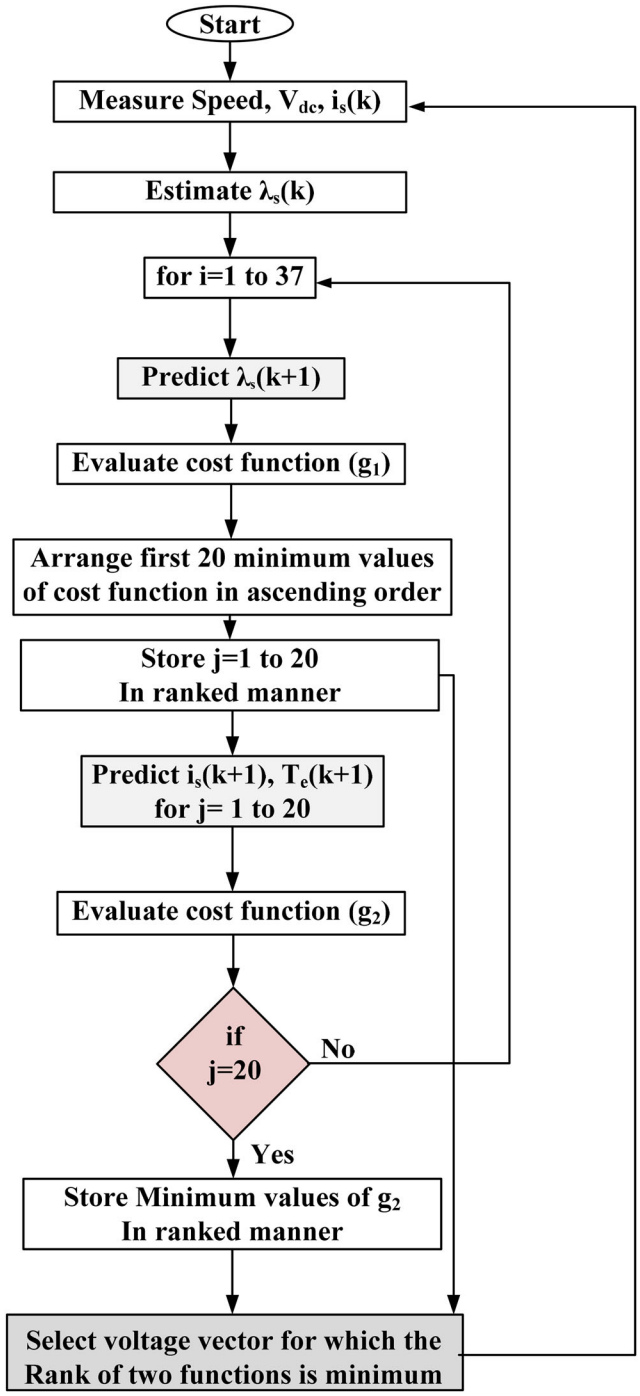

FIGURE 6. Flow chart of weighting factor eliminated PTC strategy.

Step 10: From the (21) and (22), the switching combination which gives minimum rank is chosen as the optimum voltage vector and applied in the sequential control cycle.

Figure 5 is for illustration of the effect of voltage space vectors on flux ripple. The dark portioned voltage vectors

Name of the parameter	Annotation	Quantity
Stator Resistance	R_s	4.2 Ω
Rotor Resistance	R_r	2.68 Ω
Stator Inductance	L_s	0.54 H
Rotor Inductance	L_r	0.54 H
Mutual Inductance	L_m	0.512 H
Poles	P	4
Inertia	J	0.031 kg-m^2
Line-Line Voltage	V_{rms} (L-L)	400 V
Rated Power	P_{nom}	3.7 kW
Torque	T_{nom}	24.48 N-m
Rated or Reference flux	λ_{nom} or λ_{sref}	1 Wb
Rated Speed	N_r	1440 RPM
DC- link Voltage	V_{dc}	540 V

TABLE 1. Parameters of OEWIMD used for experimental validation.

i.e. vectors V_{16} to V_{10} gives minimum flux ripple, by assuming the flux space vector is in sector-1 (in between 0° to 60° with respect to the α-axis). Another advantage of this method; it does not need sector information, for the sake of understanding only flux space vector is assumed to be in sector-1, whereas the recent PTC strategies [22] and [24] require sector or position information, therefore, the complexity gets increases.

Figure 6 represents the flow chart of the proposed PTC strategy. While developing the proposed PTC strategy, it is important to consider g_1 comprises flux error minimization and g_2 comprising torque error minimization because if the torque ripple is used in cost function g_1, then g_1 should be evaluated for 37 switching combinations. Out of these 37 combinations to reduce torque ripple there exist 22 voltage vectors then g_2 should be evaluated for 22 switching combinations. The torque error-based PTC strategy is shown in [22]. As per these articles if the torque ripple is considered in function g_1 it increases computational complexity and minimization of cost function g_2 has to be performed for 22 switching combinations rather than 20 switching combinations.

The proposed algorithm has several advantages, when compared with classical PTC and other recent PTC strategies they are as follows:

(i) The cost function is divided into g_1 and g_2, therefore, it eliminates weighting factors, and hence the effect of weighting factors is eliminated.
(ii) Cost function g_1 gives the voltage vectors that produce minimum flux ripple and the cost function g_2 delivers an optimal voltage vector that gives minimum torque ripple, therefore the obtained voltage vector can reduce flux ripple as well as torque ripple.
(iii) The cost function g_1 is evaluated for 37 combinations, whereas g_2 is evaluated and optimized only for 20 switching combinations. Therefore, the computational burden on controller reduces since the prediction of flux is easy whereas the prediction of torque involves more number of steps.
(iv) In step 4 on arranging the ascending order of voltage vectors that gives a minimum flux ripple provides another advantage *i.e.*, the voltage vectors near to another give minimum flux ripples; thereby the number of switching transitions between one voltage space vector to other voltage space vector is less, therefore switching frequency gets reduces. It does not involve additional terms in cost function to reduce switching frequency.
(v) As switching frequency reduces the common-mode voltage also gets decreases.

4. SIMULATION AND EXPERIMENTAL RESULTS

4.1. Simulation Studies

In order to verify the effectiveness of the developed PTC strategy, simulation and experimental studies are carried on OEWIMD. The specifications of OEWIMD used to simulate and also to perform experiment are shown in Table 1. After implementing the proposed PTC strategy, the obtained experimental results are compared with the classical PTC strategy. The simulated response of OEWIMD with classical and proposed PTC strategy is shown in Figure 7. Figure 7a represents the simulated response classical PTC whereas Figure 7b represents the proposed PTC. Figure 7 shows speed, torque, flux, a-phase current, a-phase voltage and CMV of OEWIMD for forward motoring to reverse motoring. Figure 7 is to describe the dynamic variation of speed from forward motoring (100 rad/s) to reverse motoring (–100 rad/s). From Figure 7, it is identified that torque and flux ripple with the proposed PTC is less. From Figure 7a and b, it is also observable that the proposed PTC provides all characteristics as that of classical PTC. In addition, it gives less switching frequency and CMV. Figure 8a represents the steady-state torque ripple of OEWIMD with classical DTC, and Figure 8b represents the proposed PTC at a speed of 125 rad/s, whereas Figure 8c and d represents flux ripple waveforms of classical and proposed PTC for visual representation of torque ripple; the zoomed portion in Figure 7 has been shown. Figure 9 demonstrates the torque, flux and currents

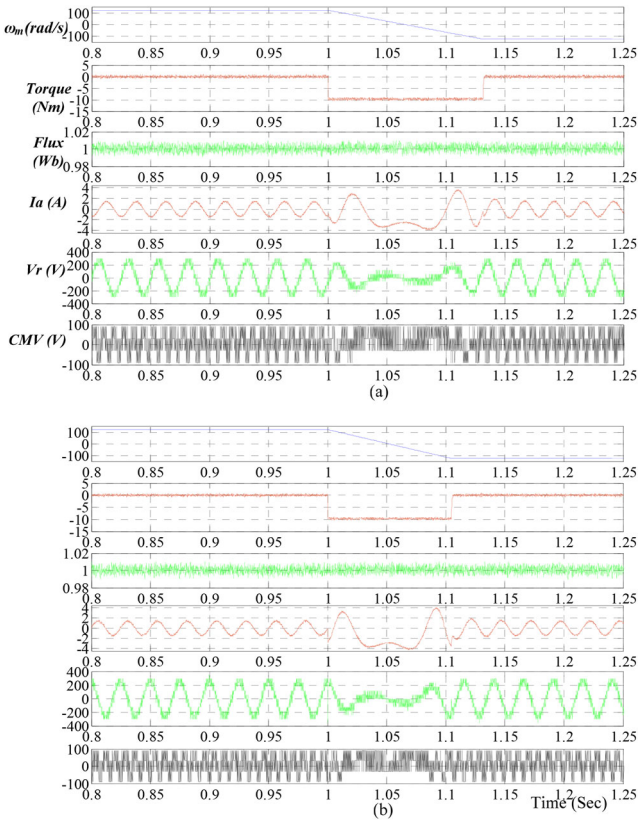

FIGURE 7. Simulated response of OEIWM drive for the speed variation from 125 rad/s to -125 rad/s: (a) Classical PTC and (b) Proposed PTC.

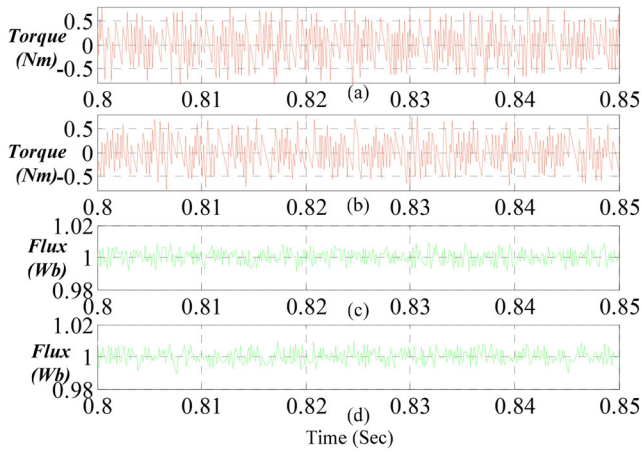

FIGURE 8. Simulated response: Torque ripple (a) Conventional PTC (b) Proposed PTC and Flux ripple (c) Conventional PTC (d) Proposed PTC.

Figure 11 demonstrates torque and flux of OEWIMD for dynamic speed variations. The OEWIMD operates with constant reference flux even if there is a speed variation from 125 rad/s to −125 rad/s. From Figure 11a and b, it is also obvious that the proposed PTC gives lesser ripples in torque and flux. Figure 12 demonstrates CMV of OEWIMD at a speed of 125 rad/s. The CMV in the proposed PTC is less when compared to classical PTC shown in Figure 12a. CMV obtained in classical PTC is 86.3 V (RMS) and CMV with proposed PTC is 75.4 V (RMS) at

under transient conditions. From Figures 8 and 9, it is evident that the proposed PTC gives less ripples in torque, flux and also shows the improved transient response.

4.2. Experimental Studies

The experimental setup used to implement the proposed PTC is shown in Figure 10. The experimental studies are performed by implementing the proposed PTC with the dSPACE-1104 controller. Speed, DC-link voltage and phase currents are sensed with transducers and these are fed back to the control algorithm by using analog to digital converters of dSPACE. From the control algorithm, switching pulses are obtained and these are provided to the inverter with the help of digital I/O pins. The experimental studies are performed for various speeds and different loading conditions; in the interest of brevity the response of OEWIMD is shown for 125 rad/s and 100 rad/s during loaded and no-load conditions. From the experimental results, the proposed PTC algorithm provides all the features of classical PTC.

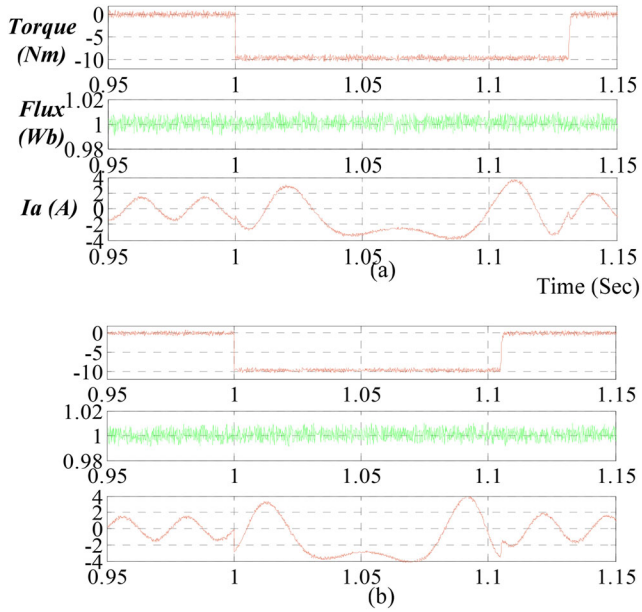

FIGURE 9. Simulated response of Torque, Flux and Current during Transient case: (a) Conventional PTC and (b) Proposed PTC.

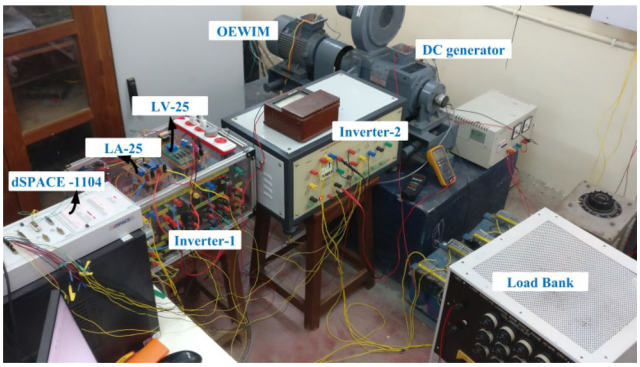

FIGURE 10. Experimental test bench.

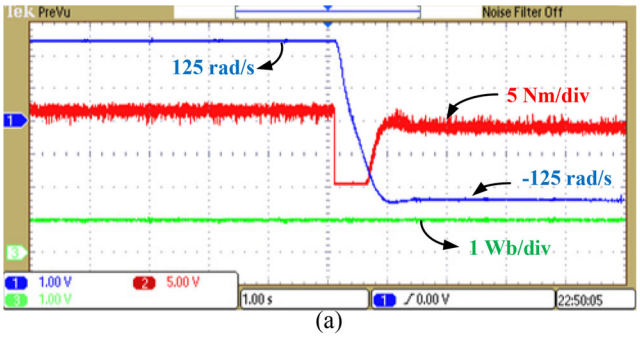

(a)

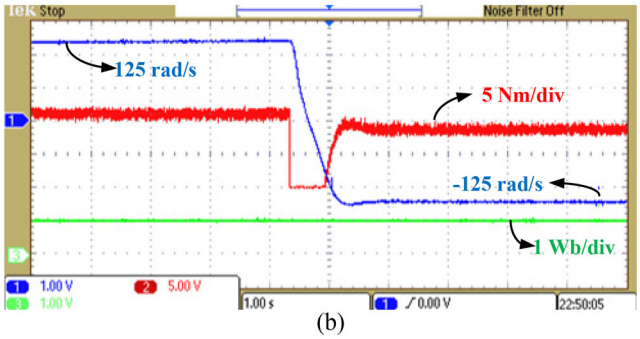

(b)

FIGURE 11. Speed, torque and flux of OEWIMD for the speed variation from 125 rad/s to -125 rad/s: (a) classical PTC and (b) Proposed PTC.

125 rad/s. Therefore, proposed PTC gives less CMV. Figure 13 presents phase voltage, phase current and voltage space vector transitions during no-load condition. From Figure 13a and b, the proposed PTC operates with less switching frequency as compared to classical PTC. The switching frequency of classical PTC is 3.23 kHz, whereas the proposed PTC operates with 2.87 kHz at 125 rad/s, hence from Figure 13 it is evident that the proposed PTC operates with low switching frequencies.

To verify the dynamic response of the proposed PTC, the OEWIMD is subjected to a sudden load torque and it

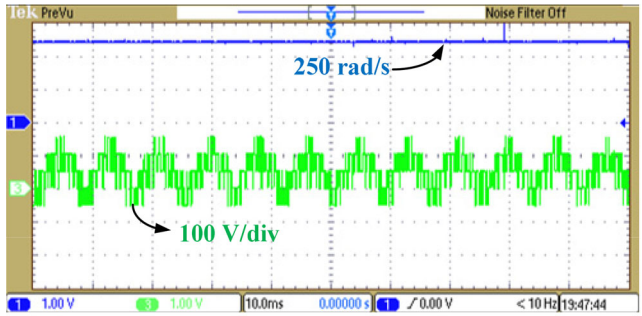

(a)

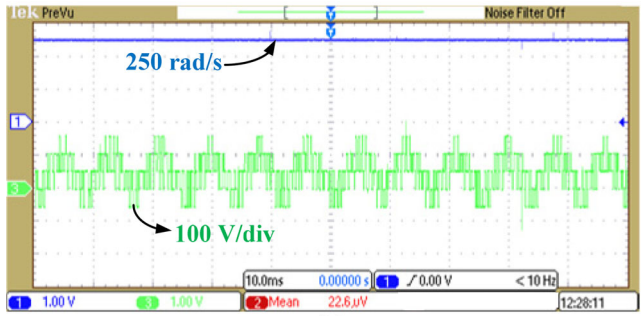

(b)

FIGURE 12. CMV of OEWIMD at a speed of 125 rad/s: (a) classical PTC and (b) Proposed PTC.

is shown in Figure 14. In Figure 14, a load torque (top figure) is applied and the zoomed portion represents phase current and load torque at 100 rad/s (bottom figure). From Figure 14, it is clearly observed that the proposed PTC gives less torque ripples and less current distortions. Figure 15 presents total harmonic distortion (THD) in phase current at a load torque of 5 Nm for the classical PTC and the proposed PTC. From Figure 15a and b, it is evident that the proposed PTC gives less THD than the classical PTC. Experimental studies are performed for various speeds of operation; for simplicity only some of the results are presented. The torque, flux ripple, switching frequency and computational time of proposed PTC were tabulated. Table 2 represents steady-state numerical ripples and distortions in current. The proposed PTC is compared with classical PTC and recent PTC techniques from (Table 2), and it is identified that the proposed gives better performance.

The ripples in torque and flux are calculated using (23).

$$\text{Ripple} = \sqrt{\left(\frac{1}{n-1}\right)\sum_{i=1}^{n}\left(k_i - \bar{k}\right)^2} \qquad (23)$$

where $\bar{k} = \frac{1}{n}\sum_{i=1}^{n} k_i$. In Eqs. (22) and (23), n indicates the number of samples and n = 1,25,000 samples.

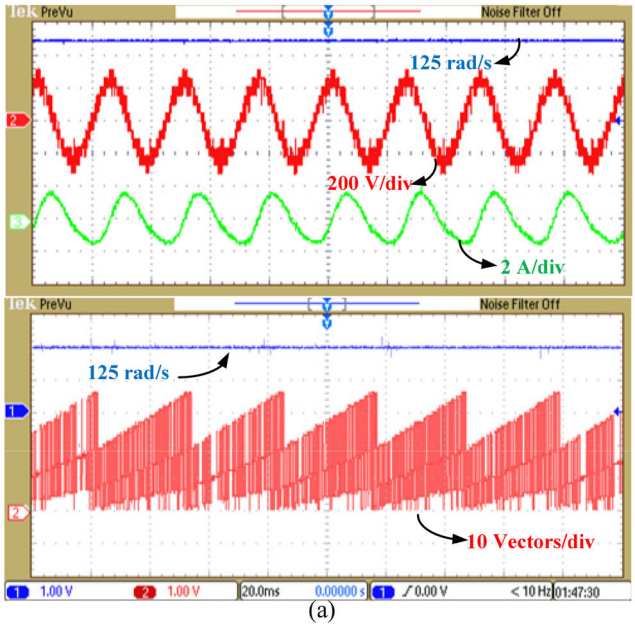

(a)

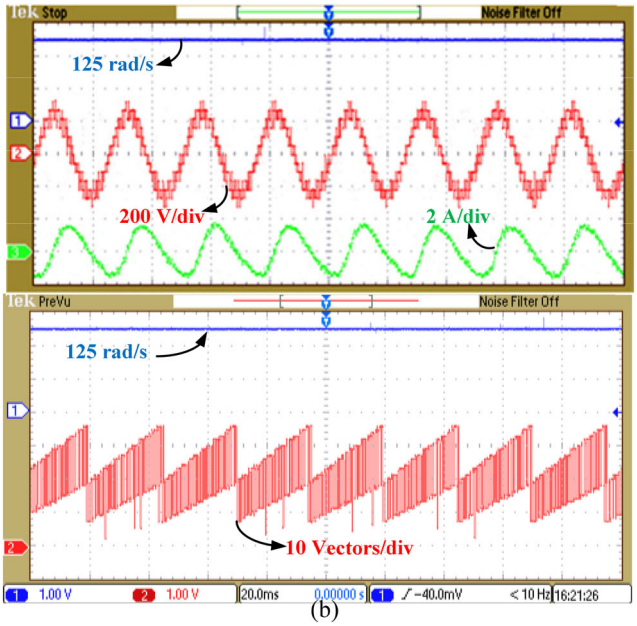

(b)

FIGURE 13. Phase voltage, phase current and space vector transitions at a speed of 125 rad/s: (a) classical PTC and (b) Proposed PTC.

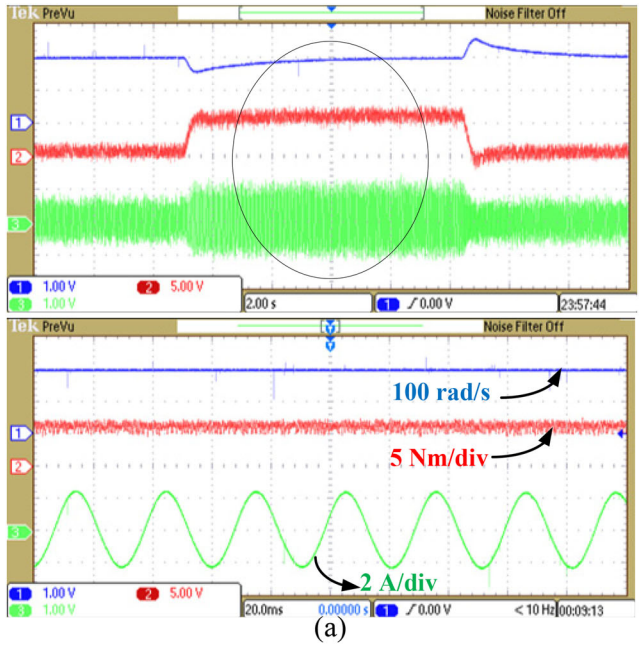

(a)

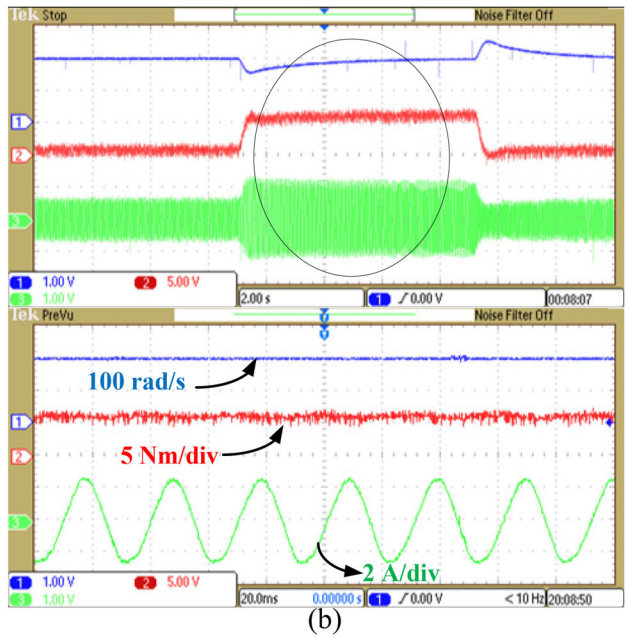

(b)

FIGURE 14. Phase current of OEIWM at a load torque of 5 Nm and speed of 100 rad/s: (a) classical PTC and (b) Proposed PTC.

The switching frequencies in classical PTC and proposed PTC are listed in Table 3. To determine the efficiency of the proposed PTC, the OEWIMD has been loaded with a load torque of 5 Nm. At a steady load torque of 5 Nm, the switching looses (P_{swL}), conduction losses (P_{cL}), have been determined. With the help of P_{swL} and P_{cL}, the total drive loss (P_L) has been obtained. With the help of shaft output power and losses of the drive, the efficiency (η) has been determined. The P_{swL}, P_{cL}, P_L and (% η) are shown in Table 3. From the losses, it is evident that the proposed PTC gives good performance than the classical PTC. After implementing the proposed PTC strategy

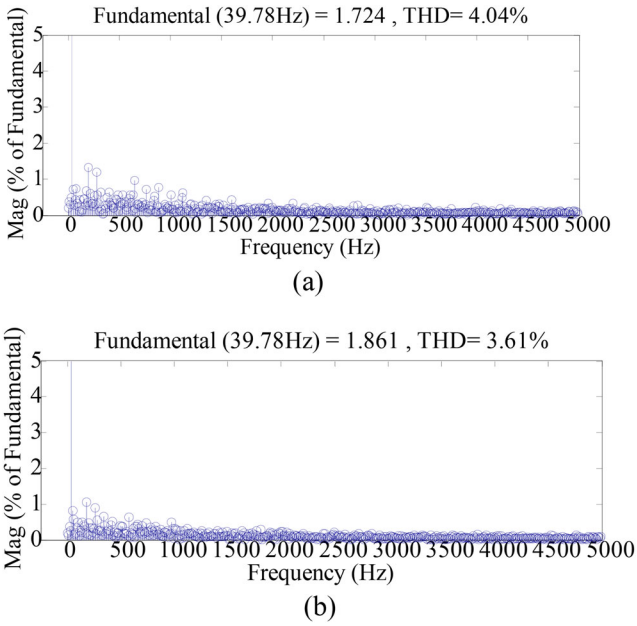

FIGURE 15. Total Harmonic Distortion in Phase current of OEIWM at a load torque of 5 Nm: (a) classical PTC and (b) Proposed PTC.

Speed (rad/s)	Classical PTC Torque ripple (Nm)	PTC [24] Torque ripple (Nm)	PTC [22] Torque ripple (Nm)	Proposed PTC Torque Ripple (Nm)
50	1.96	1.84	1.85	1.65
100	1.74	1.7	1.65	1.42
125	1.48	1.35	1.4	1.28

TABLE 2. Quantified values of steady-state average torque ripple.

and recent PTC strategies [22] and [24], it is evident that the proposed PTC is simple and easy. The complexities of [22] and [24] are as follows: estimation of flux space phasor angles of both stator and rotor, identification of flux space phasor position, sector information of flux space phasor and an additional PI controller. Table 4 demonstrates

Method	Computational Time
Classical PTC	65.5 μs
PTC [24]	58.5 μs
PTC [22]	56.4 μs
Proposed PTC	52.5 μs

TABLE 4. Computational time involved in proposed PTC in comparison with recent PTC.

computational burden of the proposed PTC strategy with respect to recent PTC strategies.

5. CONCLUSIONS

This article introduced a simplified weighting factor eliminated PTC strategy to an OEWIMD with four-level inversion. This method simplifies the cost function. The proposed PTC classifies the voltage vectors in order to reduce torque and flux ripples. The flux error is reduced by using cost function g_1 with 37 space vectors. The optimum voltage vectors obtained in cost function-I are used to reduce torque error with the help of cost function-II and it uses 20 voltage vectors. By dividing the cost function into two categories, the proposed PTC gives lesser ripples in torque and flux. The simplicity of the proposed PTC is using of the cost functions g_1 and g_2. The proposed PTC is easy to understand and implement in real time with less computational burden. It does not require complex expressions and evaluations. The proposed PTC is free from weighting factors, trigonometric equations, sector identification, pre-defined set of voltage space vectors and exact location of flux space phasor.

To verify the effectiveness of the proposed PTC strategy simulation and experimental studies are performed and these are compared with classical PTC strategy as well as recent PTC methods. From the experimental results, it is evident that the proposed PTC gives superior performance in terms of lesser ripples in torque, flux, less switching frequency, CMV and computational burden. Finally, an effective weighting factor eliminated PTC strategy has been developed to an OEWIMD in a simpler way.

Speed	Classical PTC	Proposed PTC	Classical PTC (Losses & η)				Proposed PTC (Losses & η)			
			P_{swL}(W)	P_{cL}(W)	P_L(W)	% η	P_{swL}(W)	P_{cL}(W)	P_L(W)	% η
100 rad/s	3.15 kHz	2.76 kHz	92.38	6.37	98.75	87.5	77.262	6.32	83.582	89.42
200 rad/s	3.75 kHz	3.08 kHz	77.615	6.52	84.135	89.35	53.03	6.62	59.65	92.45
250 rad/s	3.23 kHz	2.87 kHz	122.63	13.25	135.88	82.8	93.49	11.25	104.74	86.74

TABLE 3. Switching frequency, losses and % Efficiency of the proposed PTC in comparison with classical PTC.

ACKNOWLEDGEMENT

The authors would like to acknowledge the Science and Engineering Research Board (SERB) for sponsoring the project with the grant number SERB-SRG/2020/000472 and in part to SVNIT for SEED Money.

ORCID

V. Praveen Kumar Kunisetti http://orcid.org/0000-0001-7384-961X
T. Vinay Kumar http://orcid.org/0000-0002-7250-6655

REFERENCES

[1] S. Kouro, et al., "Recent advances and industrial applications of multilevel converters," *IEEE Trans. Ind. Electron.*, vol. 57, no. 8, pp. 2553–2580, Aug. 2010. DOI: 10.1109/TIE.2010.2049719.

[2] J. Rodriguez, J. S. Lai and F. Z. Peng, "multilevel inverters: a survey of topologies, controls, and applications," *IEEE Trans. Ind. Electron.*, vol. 49, no. 4, pp. 724–738, Aug. 2002. DOI: 10.1109/TIE.2002.801052.

[3] S. Lakhimsetty, N. Surulivel and V. T. Somasekhar, "Improvised SVPWM strategies for an enhanced performance for a four-level open-end winding induction motor drive," *IEEE Trans. Ind. Electron.*, vol. 64, no. 4, pp. 2750–2759, April 2017. DOI: 10.1109/TIE.2016.2632059.

[4] P. Vas, *Sensorless Vector and Direct Torque Control*, New York, Tokyo: Oxford University Press, 1998.

[5] I. Takahashi and T. Noguchi, "A new quick-response and high efficiency control strategy of an induction motor," *IEEE Trans. Ind. Appl.*, vol. IA-22, no. 5, pp. 820–827, 1986. DOI: 10.1109/TIA.1986.4504799.

[6] D. Rekioua and T. Rekioua, "DSP-controlled direct torque control of induction machines based on modulated hysteresis control," in 2009 International Conference on Microelectronics - ICM, 2009, pp. 378–381, DOI: 10.1109/ICM.2009.5418603.

[7] J. Rodriguez and P. Cortes, *Predictive Control of Power Converters and Electrical Drives*, Chichester, United Kingdom: John Wiley-IEEE, 2012.

[8] Y. Zhang and H. Yang, "Generalized two-vector-based model-predictive torque control of induction motor drives," *IEEE Trans. Power Electron.*, vol. 30, no. 7, pp. 3818–3829, Jul. 2015. DOI: 10.1109/TPEL.2014.2349508.

[9] P. Karamanakos, P. Stolze, R. M. Kennel, S. Manias and H. D. T. Mouton, "Variable switching point predictive torque control of induction machines," *IEEE J. Emerg. Sel. Topics Power Electron.*, vol. 2, no. 2, pp. 285–295, Jun. 2014. DOI: 10.1109/JESTPE.2013.2296794.

[10] I. Osman, D. Xiao, K. S. Alam, S. M. S. I. Shakib, M. P. Akter and M. F. Rahman, "Discrete space vector modulation-based model predictive torque control with no sub-optimization," *IEEE Trans. Ind. Electron.*, vol. 67, no. 10, pp. 8164–8174, Oct. 2020. DOI: 10.1109/TIE.2019.2946559.

[11] M. R. Nikzad, B. Asaei and S. O. Ahmadi, "Discrete duty-cycle-control method for direct torque control of induction motor drives with model predictive solution," *IEEE Trans. Power Electron.*, vol. 33, no. 3, pp. 2317–2329, March 2018. DOI: 10.1109/TPEL.2017.2690304.

[12] T. Wang, C. Liu, G. Lei, Y. Guo and J. Zhu, "Model predictive direct torque control of permanent magnet synchronous motors with extended set of voltage space vectors," *IET Electric Power Appl.*, vol. 11, no. 8, pp. 1376–1382, Sept. 2017. DOI: 10.1049/iet-epa.2016.0870.

[13] Z. Li, J. Xia, Y. Guo and X. Zhang, "Fault-Tolerant predictive torque control design for induction motor drives based on discrete space vector modulation," *IEEE J. Emerg. Sel. Topics Power Electron.*, vol. 9, no. 5, pp. 5441–5451, Oct. 2021. DOI: 10.1109/JESTPE.2021.3064979.

[14] Y. Zhang, B. Zhang, H. Yang, M. Norambuena and J. Rodriguez, "Generalized sequential model predictive control of IM drives with field-weakening ability," *IEEE Trans. Power Electron.*, vol. 34, no. 9, pp. 8944–8955, Sept. 2019. DOI: 10.1109/TPEL.2018.2886206.

[15] C. Ma, et al., "A novel torque boundary-based model predictive torque control for PMSM without weighting factor," *IEEE J. Emerg. Sel. Topics Power Electron.*, vol. 9, no. 4, pp. 4395–4406, Aug. 2021. DOI: 10.1109/JESTPE.2020.3039687.

[16] X. Lin, W. Huang, W. Jiang, Y. Zhao and S. Zhu, "Predictive torque control for PMSM Based on weighting factor elimination and fast voltage vector selection," *IEEE J. Emerg. Sel. Topics Power Electron.*, vol. 8, no. 4, pp. 3736–3750, Dec. 2020. DOI: 10.1109/JESTPE.2019.2937194.

[17] K. V. Praveen Kumar and T. V. Kumar, "Predictive torque control of open-end winding induction motor drive fed with multilevel inversion using two two-level inverters," *IET Electric Power Appl.*, vol. 12, no. 1, pp. 54–62, 2018. DOI: 10.1049/iet-epa.2017.0209.

[18] K. V. Praveen Kumar and T. V. Kumar, "Enhanced predictive torque control of multi-level inverter fed open-end winding induction motor drive based on predictive angle control," *EPE J.*, vol. 30, no. 2, pp. 94–104, 2020. DOI: 10.1080/09398368.2020.1733306.

[19] M. Habibullah, D. D. C. Lu, D. Xiao, I. Osman and M. F. Rahman, "Selected prediction vectors based FS-PTC for 3L-NPC inverter fed motor drives," *IEEE Trans. Ind. Appl.*, vol. 53, no. 4, pp. 3588–3597, July-Aug. 2017. DOI: 10.1109/TIA.2017.2677362.

[20] D. Xiao, K. S. Alam, I. Osman, M. P. Akter, S. M. S. I. Shakib and M. F. Rahman, "Low complexity model predictive flux control for three-level neutral-point clamped inverter-fed induction motor drives without weighting factor," *IEEE Trans. Ind. Appl.*, vol. 56, no. 6, pp. 6496–6506, Nov-Dec. 2020. in DOI: 10.1109/TIA.2020.3016617.

[21] X. Zhang and W. Zhang, "Model predictive full-torque control for the open-winding PMSM system driven by dual inverter with a common DC bus," *IEEE J. Emerg. Sel.*

Topics Power Electron., vol. 9, no. 2, pp. 1541–1554, April 2021. DOI: 10.1109/JESTPE.2020.2980678.

[22] R. E. Kodumur Meesala, V. P. K. Kunisetti and V. Kumar Thippiripati, "Enhanced predictive torque control for open end winding induction motor drive without weighting factor assignment," *IEEE Trans. Power Electron.*, vol. 34, no. 1, pp. 503–513, Jan. 2019. DOI: 10.1109/TPEL.2018.2812760.

[23] K. M. R. Eswar, K. V. P. Kumar and T. V. Kumar, "A simplified predictive torque control scheme for open-end winding induction motor drive," *IEEE J. Emerg. Sel. Topics Power Electron.*, vol. 7, no. 2, pp. 1162–1172, Jun. 2019. DOI: 10.1109/JESTPE.2018.2832240.

[24] M. Habibullah, D. D. C. Lu, D. Xiao, J. E. Fletcher and M. F. Rahman, "Low complexity predictive torque control strategies for a three-level inverter driven induction motor," *IET Electric Power Appl.*, vol. 11, no. 5, pp. 776–783, 2017. DOI: 10.1049/iet-epa.2016.0572.

[25] M. R. Zamani, Z. Rahmani and B. Rezaie, "A novel model predictive control for a piecewise affine class of hybrid system with repetitive disturbance," *ISA Trans.*, vol. 108, pp. 18–34, 2021. DOI: 10.1016/j.isatra.2020.08.023.

[26] M. R. Zamani, Z. Rahmani and B. Rezaie, "A novel framework of model predictive control for controlling a class of nonlinear system in the presence of uncertainty," *J. Vibration Control*, vol. 28, no. 11-12, pp. 1279–1294, Feb. 2022. DOI: 10.1177/1077546321990179.

[27] M. R. Zamani, Z. Rahmani and B. Rezaie, "A novel model predictive control strategy for constrained and unconstrained systems in presence of disturbance," *IMA J. Math. Control Information*, vol. 37, no. 1, pp. 208–225, Mar. 2019. DOI: 10.1093/imamci/dny046.

BIOGRAPHIES

V. Praveen Kumar Kunisetti received the B.Tech and M.Tech degrees in Electrical Engineering from Jawaharlal Nehru Technological University Kakinada, India, in 2011 and 2014, respectively and the Ph.D. Degree in Electrical Engineering from the National Institute of Technology, Warangal, India in 2019. In 2019, he joined in the Department of Electrical Engineering, Sardar Vallabhbhai National Institute of Technology, Surat as an Assistant Professor. His research interests include power electronics and drives, multi-level inverters, predictive control, open-end winding motor drives, hybrid electric vehicles and renewable energy interfacing.

Vinay Kumar Thippiripati was born in Kadapa, India, in 1984. He received the B.Tech and M.Tech Degrees in Electrical Engineering from Jawaharlal Nehru Technological University, Hyderabad, India in 2005 and 2008, respectively. He received the Ph.D. Degree in Electrical Engineering from the National Institute of Technology, Warangal, India, in 2015. In 2013, he joined as an Assistant Professor in the Department of Electrical Engineering in National Institute of Technology, Warangal. His research interests include power electronics and drives, multi-level inverters, direct torque control, predictive torque control, open-end winding induction motor drives, hybrid electric vehicles and renewable energy interfacing.